Diffusion and Drift Reduction in Artificial Cells

Ryan Smolarsky

December 12, 2022

Faculty Advisor: Viva Horowitz

Hamilton College

Department of Physics

Submitted as a Partial Requirement for the Senior Project

Abstract

The goal of the artificial cells project is to construct an artificial cytoplasm where molecular motion comparable to what is observed in a biological cell can both be observed and analyzed. The current study contributes to this project by attempting to create a readily repeatable drift-reducing chamber by modifying the methods used by Palacci (2010)[1] and by studying the passive diffusion of tracer particles in media containing various combinations of different polyethylene glycol (PEG) concentrations and polymer chain lengths. The drift-reducing chamber section of this study used an agarose hydrogel inside of a perfusion chamber to construct prototypes. A prototype was constructed such that a seal where no tracer particles could enter or exit the interior of the hydrogel well. These results regarding the drift-reducing chamber suggest that such a repeatable and effective chamber can be constructed. In the second section of this study pertaining to diffusion analysis, it was demonstrated that the diffusion coefficient decreased with either an increased PEG concentration or increased PEG polymer chain length. Additionally, the diffusive exponent remained constant at $\alpha = 1$, demonstrating a clear difference from fueled motion[2,3]. The results from the diffusion analysis section of this study demonstrate the effects that may be observed in a more crowded medium, such as the intracellular environment.

[1] Palacci, J., *Manipulation of colloids by osmotic forces*. 2010, Université Claude Bernard-Lyon I.
[2] Horowitz, V.R., et al., *Active colloidal particles in emulsion droplets: a model system for the cytoplasm.* The European Physical Journal Special Topics, 2019. **227**(17): p. 2413-2424.
[3] Howse, J.R., et al., *Self-Motile Colloidal Particles: From Directed Propulsion to Random Walk.* Physical Review Letters, 2007. **99**(4): p. 048102.

1 CONTENTS

2 ACKNOWLEDGEMENTS

I would like to express my gratitude to Professor Viva Horowitz for allowing me to be her thesis student this semester. Her role as an advisor in the undertaking of this thesis cannot be overstated and she was integral to the work done during this project, both through her enduring support during my time with this project and her efforts in this field prior to my involvement.

I would also like to express my gratitude to Elizabeth Seider for all her help in the lab over the course of the semester. After injuring my thumb, most lab techniques were impossible for me to perform on my own and without her experimental contributions, the work accomplished during this project would not have been possible. Her contributions to this project over the course of this semester are greatly appreciated.

I'd also like to extend my thanks to several professors in the physics department who have contributed to my education in physics during my time at Hamilton College – Professor Gordon Jones (especially because of his help as my faculty advisor), Professor Seth Major, and Professor Brian Collett.

I'd also like to mention all those in my personal life that have supported me throughout my education while at Hamilton College: my mother, father, and sister for their love, support, and encouragement throughout my studies, and also my friends and fellow physics concentrators who I have spent many hours with over these past four years in our studies – especially Ryan Hunt, Jacob Sichlau, Liam Regan, and Lance Barton, among many others.

I would not be where I am today without all those mentioned and others not included here, and I greatly appreciate all their involvements in my academic career and life.

3 INTRODUCTION

3.1 BACKGROUND – TRACER DIFFUSION

The cytoplasm of a biological cell is a crowded environment, full of organelles, proteins, and many other types of biomolecules. Many molecules within the intracellular environment move by passive diffusion. Also known as Brownian motion, passive diffusion is the random motion of particles in a medium. Other molecules travel through the intracellular environment via energetic processes such as active transport, an example of which is the movement of motor proteins [1].

Many previous studies include observations of the passive diffusion of particles in various environments [2-4]. Many of these studies focus on the analysis of passive diffusion in artificially made environments, such as colloidal suspensions [2] and lattice gases [3, 4]. One such study observing diffusion in colloidal suspensions uses an optical property known as the structure factor to deduce parameters characterizing the diffusive motion of tracer particles within the medium [2]. Studies involving lattice gases, which are simulated groups of atoms that must remain in a bounded space [5], use these simulations to mimic a fluid environment that can be tuned to have specific characteristics, such as changing the identity of the atoms in the lattice [3, 4].

Another branch of diffusion studies focus on the observation of tracer particles in biological media, such as extracellular and intracellular environments [6, 7]. One study by Leptos et al. (2009) [6] focuses on tracer particle diffusion in suspensions with eukaryotic alga cells, demonstrating that the presence of biological cells can affect the motion of inert tracer particles in an extracellular environment. One study has also measured relative diffusion coefficients of tracer particles in an intracellular environment of biological cells [7]. In this study, Luby-Phelps et al. (1987) [7] varied the radius of tracer particles and measured their relative diffusion coefficients in the cytoplasm of

fibroblast cells. They found that with an increased tracer particle radius, the relative diffusion coefficient in the cytoplasm strongly decreased [7].

3.2 Background – Drift-Reducing Chamber

Both in the study of passive particle diffusion and active, fueled particle motion, ensemble drift is a glaring source of error that can prevent the collection of reliable data [1, 8]. A study by Palacci (2010) [8] includes instructions for the construction of a drift-reducing chamber – however, these methods are difficult to repeat.

Drift presents an issue in the collection of data regarding passive diffusion, but even more so with data pertaining to fueled particle motion. Horowitz et al. (2019) [1] and Howse et al. (2007) [9] observed this superdiffusive fueled motion using Janus particles, which are fluorescently dyed sulfate latex particles that are half-coated with platinum. This platinum catalyzes a decomposition reaction of hydrogen peroxide, resulting in water and molecular oxygen [1, 9]:

$$2H_2O_2 \xrightarrow{Pt} 2H_2O + O_2 \quad (1)$$

This reaction produces a gradient of dissolved molecular oxygen, allowing Janus particle self-propulsion via self-diffusiophoresis [1]. These Janus particles are exciting because of the potential they have for mimicking the active transport observed in biological cells – however, the production of molecular oxygen poses a significant issue in the production of sample drift, as the produced oxygen can seed gaseous oxygen bubbles that can grow, merge with each other, and move about the sample [1]. Additionally, the samples must provide a way to vent the excess oxygen, but leaving the samples open to the environment allows evaporation, which also contributes to drift.

The drift-reducing chamber of Palacci (2010) [8] uses an agarose hydrogel to introduce hydrogen peroxide fuel to the particles inside the hydrogel while removing molecular oxygen from the system, simultaneously keeping the particles isolated from the motion of the external environment. An agarose hydrogel is a promising choice because of its characteristic structure, known in biology and chemistry for its ability to separate particles with different qualities through various types of gel electrophoresis. The pores in the agarose hydrogel matrix are large enough to allow molecular oxygen, water, and hydrogen peroxide to diffuse through, but are too small to allow the tracer particles or Janus particles to leave from inside of the hydrogel. This also provides the benefit that the concentration of hydrogen peroxide will be renewed during measurements instead of being exhausted over time. Despite the clear advantages of this apparatus, Palacci's design [8] is challenging to construct, due to methods requiring the drilling of glass slides and screwing these together in such a way that they surround the agarose hydrogel without the glass snapping.

3.3 GOALS OF THIS STUDY

The ultimate goal of this research is to continue the work that has been performed in the fields of passive diffusion and fueled particle motion alongside drift reduction to build an artificial system that functions similarly to that of a living cell, with the intricacies of the intracellular environment. The ability to distinguish between these two types of motion would be significantly beneficial in the study of biomolecular motion in the cytoplasm.

One specific goal of this study is to build upon previous research in the field by attempting to artificially replicate the crowdedness of the intracellular environment using various concentrations and polymer chain lengths of polyethylene glycol (PEG) **[Figure 1]**. This molecule is particularly

interesting because of its structure and composition as an organic polymer [10]. Its long chain structure and polarity make it a potential analog for intracellular biomolecules such as various types of lipids and proteins. Using PEG at various concentrations and polymer chain lengths and comparing these results to previously published findings, this study will demonstrate specifically how the crowdedness of a medium affects the passive diffusion of particles and how this differs from active, fueled motion. This comparison will allow for the distinction between passive and active motion in intracellular environments.

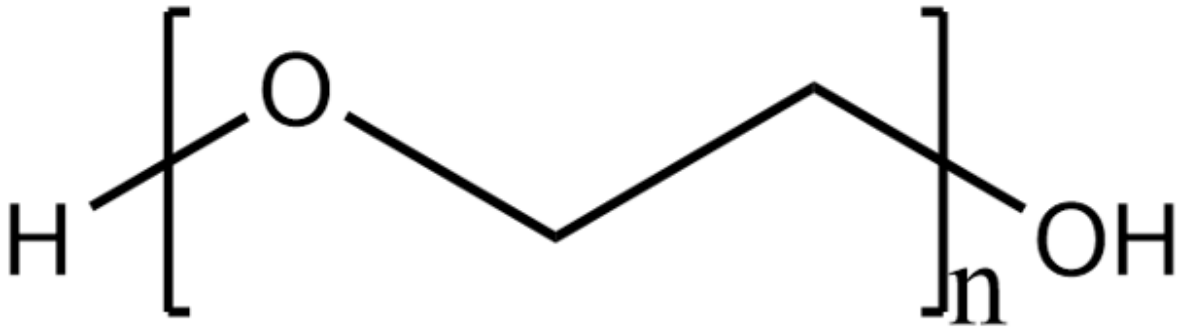

Figure 1. Polyethylene glycol (PEG), an organic polymer of various potential chain lengths. Its structure and characteristics make it a potential analog for the biomolecules found in the cell that contribute to the crowdedness of the intracellular environment.

Another rationale behind the addition of PEG into samples is to study the coupling of fueled particle motion to inert tracer particles. Horowitz et al. (2019) [1] demonstrates that the motion of inert tracer particles was not increased due to the presence of fueled Janus particle swimmers in the medium. However, this is not what is observed in the intracellular environment – according to Guo et al. (2014) [11], tracer particles put into the cytoplasm demonstrated increased diffusive motion relative to passive diffusion as a result of coupling interactions with molecular motors. The addition of molecular analogs such as PEG in sample diffusive media may allow for the

observation of coupling between tracer particles and Janus particles due to the long chain structure of PEG being able to bridge the distances between Janus particles and tracer particles.

A further goal of this study is to attempt the construction of a drift-reducing chamber with the same concept as Palacci (2010) [8] with variations to make its construction readily repeatable. Such a chamber would allow for not only consistently reliable measurements of fueled particle motion but would also make this possible in the presence of conditions comparable to those observed in the cytoplasm while avoiding drift. It would also allow for future studies to investigate potential coupling effects between fueled Janus particle motion and inert tracer particle motion.

4 THEORY

4.1 THE EINSTEIN RELATION

The theory behind diffusion must be discussed prior to describing and analyzing the diffusive motion of particles in an artificial cytoplasm. Consider a region where for some collection of particles, its concentration increases uniformly in one direction. Fick's second law describes the diffusion of particles across some surface in this region [12], such that

$$\frac{\partial n}{\partial t} = D\frac{\partial^2 n}{\partial x^2} \tag{2}$$

where n is the concentration of particles, t is the time, D is the diffusion coefficient, and x is a distance. Einstein determined the solution to this partial differential equation [13] to be

$$n(x,t) = \frac{N}{\sqrt{4\pi Dt}} e^{-\frac{x^2}{4Dt}} \tag{3}$$

where N is the number of particles diffusing about in the medium. This solution has the form of a Gaussian curve, which has a general form of

$$f(u) = Ce^{-\frac{u^2}{\sigma^2/2}} \tag{4}$$

where $f(u)$ is the general Gaussian curve function, C is some constant, u is the variable input to the function, and σ^2 is the variance of the function. Thus, the variance of Einstein's solution [13] can be determined by halving the denominator of the exponent, such that

$$\sigma_x^2 = 2Dt \tag{5}$$

where σ_x^2 is the variance of the solution in **Equation 3** with respect to displacement. The physical interpretation of this variance is the square of the average displacement a particle has traveled from

its starting position in one dimension. Thus, this variance with respect to x is simply the mean-square displacement (MSD), resulting in the Einstein relation for MSD [13]:

$$\langle x^2 \rangle = \sigma_x^2 = 2Dt \tag{6}$$

where $\langle x^2 \rangle$ is the MSD in one dimension. This same reasoning would follow in two added dimensions y and z, such that the MSD in each of these dimensions are $\langle x^2 \rangle = \langle y^2 \rangle = \langle z^2 \rangle = 2Dt$. Thus, the overall MSD in three dimensions is

$$\langle r^2 \rangle = \langle x^2 \rangle + \langle y^2 \rangle + \langle z^2 \rangle = 6Dt \tag{7}$$

where $\langle r^2 \rangle$ is the MSD in three dimensions. By the same reasoning, the two-dimensional MSD would be $4Dt$.

4.2 The Stokes-Einstein Relation

Fick's first law describes the flux across the surface mentioned above in this region [12], such that

$$J_x = -D\frac{\partial n}{\partial x} \tag{8}$$

where J_x is the flux across the surface in one dimension. From this, Einstein derives a relation for the diffusion coefficient using Stokes' Law [13], such that

$$D = \frac{RT}{6\pi N_A a \eta} \tag{9}$$

where R is the gas constant, T is the temperature, N_A is Avogadro's number, a is the particle radius, and η is the viscosity of the medium. **Equation 9** is known as the Stokes-Einstein relation [14]. This relation demonstrates that with assumptions of a constant temperature and that all diffusing particles have the same radius, the only particle that affects the diffusion coefficient and thus a particle's MSD is the medium's viscosity.

4.3 Anomalous Diffusion

Fick's laws are intended for isotropic fluids – fluids that have the same properties in all directions [14]. However, in the intracellular environment, particles diffuse through a complex medium that cannot be assumed to be isotropic [14]. In more complex environments, empirical data can be approximated using a power law built from **Equation 7** [1, 14], such that

$$\langle r^2 \rangle = 6Dt^{\alpha} \tag{10}$$

where α is the diffusive exponent that carries information about the type of diffusion observed in a sample. Normal diffusion is observed when $\alpha = 1$, resulting in the Stokes-Einstein relation [13, 14]. Anomalous diffusion is observed when $\alpha \neq 1$, which demonstrates a deviation from the Stokes-Einstein relation [14]. There are three main types of anomalous diffusion – subdiffusion, which occurs when $\alpha < 1$ [14]; superdiffusion, which occurs when $1 < \alpha < 2$ [1, 14]; and ballistic motion, which occurs when $\alpha = 2$ [1]

5 EXPERIMENTAL DESIGN – DRIFT-REDUCING CHAMBER

5.1 APPARATUS

The drift-reducing chamber **[Figure 2a-b]** consists of an agarose hydrogel with a well in its middle atop a glass slide. A perfusion chamber (Electron Microscopy Sciences) covers the hydrogel and seals to the glass slide beneath. Inside the well is the sample solution, while the excess space inside the perfusion chamber is filled with water. Imaging of the hydrogel and particles during testing was performed using either bright-field microscopy or fluorescence microscopy using a Nikon Ti-E Inverted Microscope and a ThorLabs color camera, recording data at 17.29 frames per second (fps).

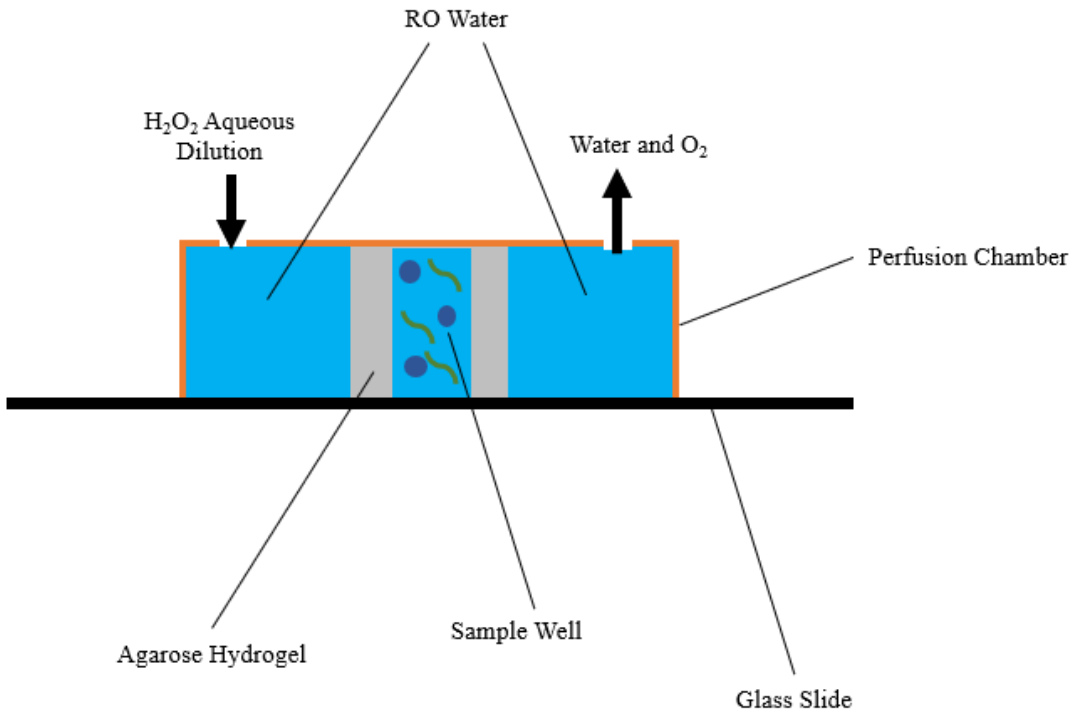

Figure 2a. Side view of the drift-reducing chamber constructed. An agarose hydrogel is placed on top of a glass slide, with the perfusion chamber sealed to the glass slide while covering the gel. RO water fills the excess space inside the chamber. There are two holes – one where an aqueous dilution of hydrogen peroxide (H_2O_2) can be input into the system and one where water and produced molecular oxygen can leave the system. [Not to scale]

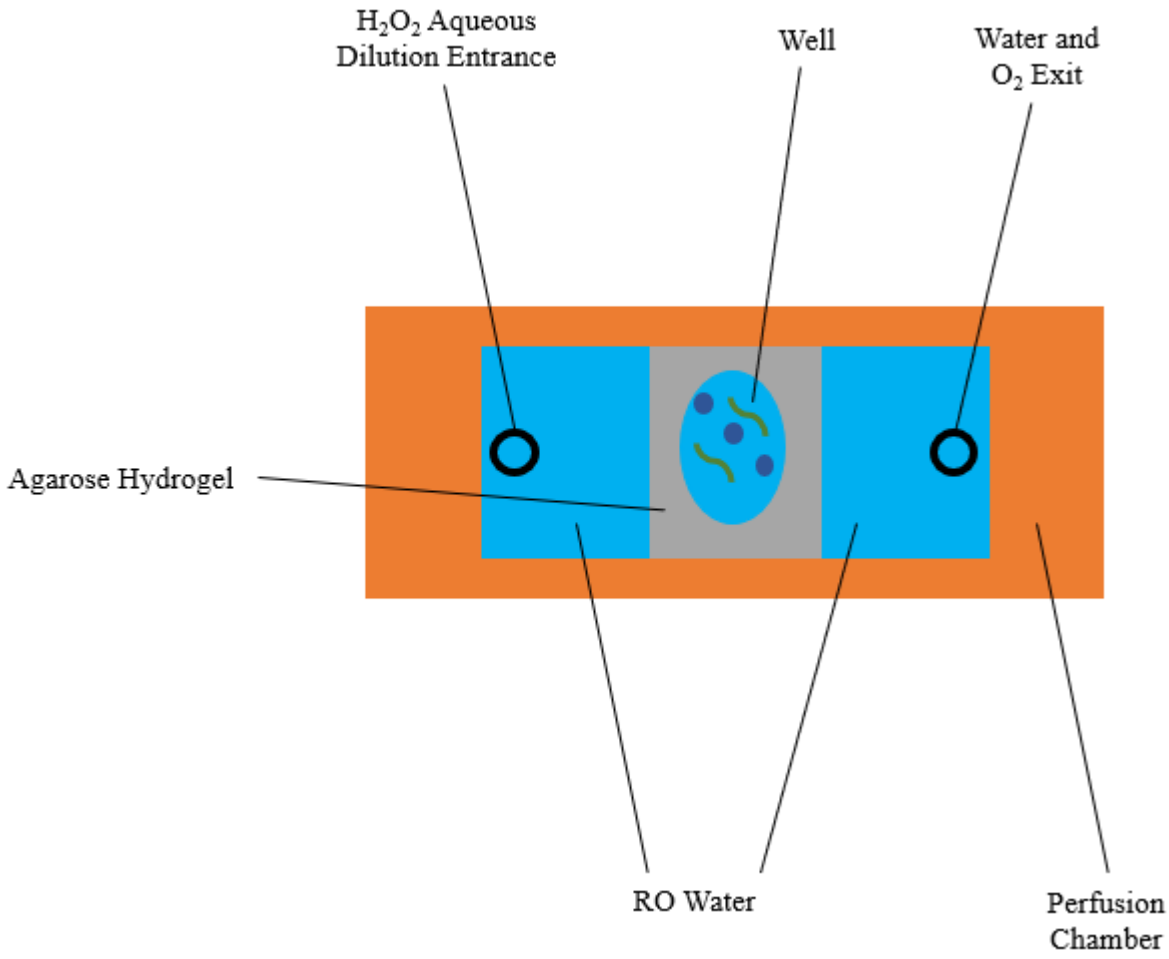

Figure 2b. Top-down view of the drift-reducing chamber constructed. The agarose hydrogel has a well cut out in its middle, where the desired sample solution can be pipetted. The perfusion chamber covers the agarose hydrogel, with RO water filling the excess space of the chamber. There is a hole where an aqueous dilution of hydrogen peroxide (H_2O_2) can be input and one hole for water and produced molecular oxygen removal. [Not to scale]

5.2 METHODS

Construction of the drift-reducing chamber began with agarose hydrogel preparation. 2.37 g of agarose powder was added to 50 mL of RO water, within the agarose concentration range of 4.5-5% w/v recommended by Palacci (2010) [8]. This mixture was vortexed for 30 seconds until it appeared as a cloudy suspension and then was microwaved at 1.35 kW for roughly 30 seconds until

boiling. The solution was stirred thoroughly and then microwaved again for 30 more seconds, resulting in a homogeneous solution of agarose and RO water.

This homogeneous solution was poured into a beaker on a hotplate at roughly 85°C with a stir bar. The beaker was covered with foil to limit evaporation and the settling of agarose at the surface [8]. Once completely stirred, the liquid hydrogel was poured into a mold and the hydrogel matrix was allowed to set by cooling to room temperature. Palacci (2010) [8] stored agarose hydrogels in aqueous environments, but it was found in the current study that settled hydrogel can be stored dry. When stored dry, previously set agarose hydrogel can be moved to a beaker and microwaved for roughly 30 seconds until it has melted and is boiling. This beaker can be placed on a hotplate, and the same molding process from this point on can be repeated to obtain a suitable agarose hydrogel. Molded hydrogels were stored in petri dishes containing RO water, whereas excess hydrogel was stored dry. Both of which were refrigerated at 2-8°C. It is unknown if storing hydrogels dry alters their properties.

The agarose hydrogel mold that was preferred by the end of the study was a brick of plastic with circular divots drilled in at various depths, as depicted in **Figure 3a-b**. Depths of 1.53 mm, 1.54 mm, 1.55 mm, 1.56 mm, 1.57 mm, 1.65 mm, 1.75 mm, 1.85 mm, and 2.05 mm were tested to determine the agarose hydrogel height that would effectively seal the interior well of the hydrogel. Molds with diameters of 0.50 inches and 1.00 inches were both tested. Once the hydrogel was set and molded, it was removed from the mold and then trimmed with a scalpel so the gel would fit within the perfusion chamber. The scalpel was also used to cut a well in the middle of the hydrogel to house the sample solution. The trimmed hydrogel was then put on a glass slide and fluorescently dyed sulfate latex tracer particles (Fluoromax, 1.1 μm diameter) were pipetted into the well. The hydrogel was then covered with the perfusion chamber, sealing the sample from the outside

environment. Through a hole on top of the perfusion chamber, RO water was pipetted into the excess space until the entire perfusion chamber was filled.

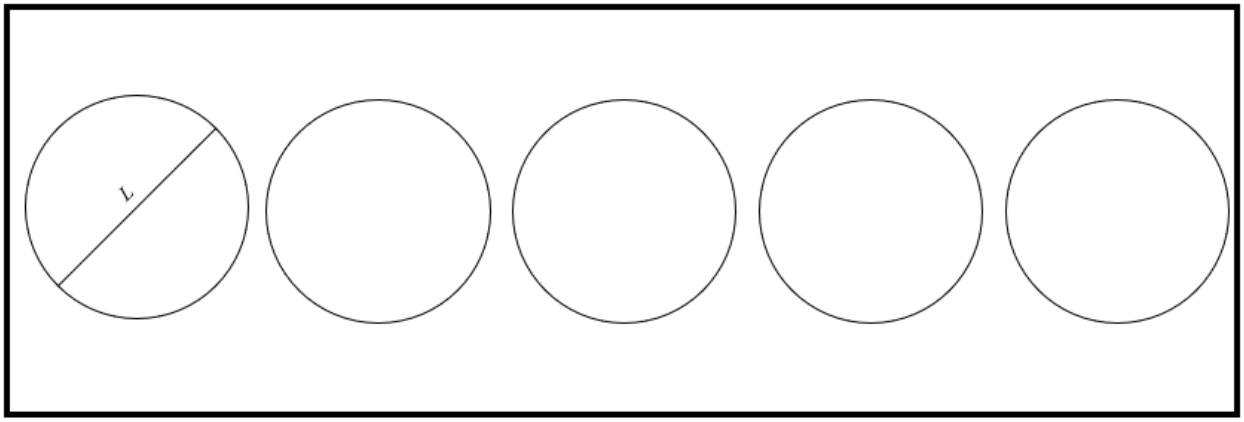

Figure 3a. Top-down view of the plastic molds used to set the agarose hydrogels. The circular divots were made with various depths, depending on the hydrogel height that was being tested. Molds had a diameter *L*, which varied over the course of the study.

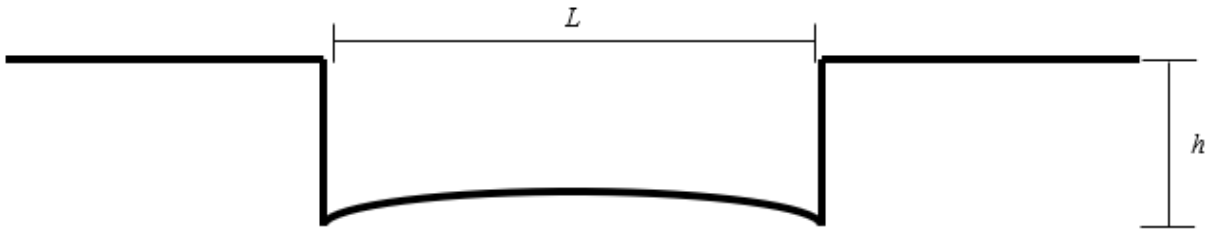

Figure 3b. Side view of the plastic mold well used to set the agarose hydrogels. The well depth, *h*, was varied throughout the study to determine an effective hydrogel height that would seal the well interior. Molds had a diameter *L* that varied over the course of the study.

Note:
The curved shape at the bottom of the mold resulted from the machining process. A slower machining process could create a flat-bottom well.
~Viva

Once the sample was prepared, it was first imaged using bright-field microscopy, followed by fluorescent microscopy. Bright-field microscopy was used to locate the boundaries of the well, while fluorescent microscopy was used to determine particle locations. The locations of particles allowed for determining whether the agarose hydrogel sealed the interior well by spanning the entire vertical space of the perfusion chamber.

6 RESULTS – DRIFT-REDUCING CHAMBER

6.1 LOCATING THE WELL BOUNDARY

Drift-reducing chamber prototypes were made using agarose hydrogels with a concentration of 4.5-5% w/v dry agarose powder. These prototypes were imaged with tracer particles inside the hydrogel well using bright-field microscopy first to determine the bounds of the well, followed by fluorescence microscopy to locate tracer particles. An example of the hydrogel well boundary is depicted in **Figure 4**.

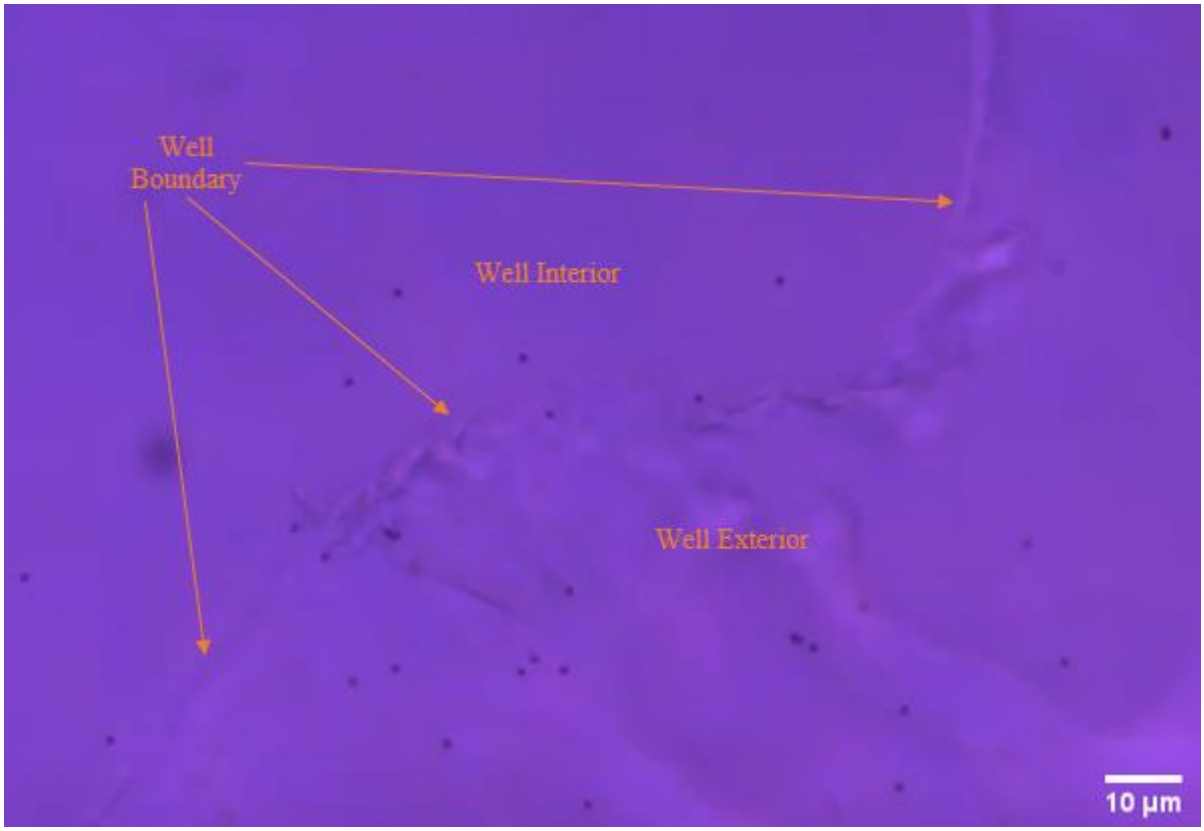

Figure 4. Bright-field microscope image of a 1.75 mm tall agarose hydrogel well boundary using 20x magnification.

6.2 TESTING DIFFERENT AGAROSE HYDROGEL HEIGHTS

Various agarose hydrogel heights (1.53 mm, 1.54 mm, 1.55 mm, 1.56 mm, 1.57 mm, 1.65 mm, 1.75 mm, 1.85 mm, and 2.05 mm) were tested in the chamber prototypes to determine which height would effectively seal the well interior. All these hydrogel heights except for 2.05 mm proved ineffective due to the hydrogel being too short to seal the well within the perfusion chamber. In the cases of hydrogels that proved ineffective, the water that filled the excess space in the chamber caused the hydrogel to float, allowing the particles in the well to leak into the rest of the perfusion chamber.

Despite the inefficacy of many hydrogel heights, promising results were obtained with the testing and imaging of the prototype with a 2.05 mm tall agarose hydrogel. With this height, the outside tallest portion of the hydrogel formed a seal that did not allow tracer particles to cross over from the exterior to the interior by contacting the cover of the perfusion chamber. **Figure 5** is a diagram that breaks down what is depicted in **Figure 6** and **Figure 7a-b**.

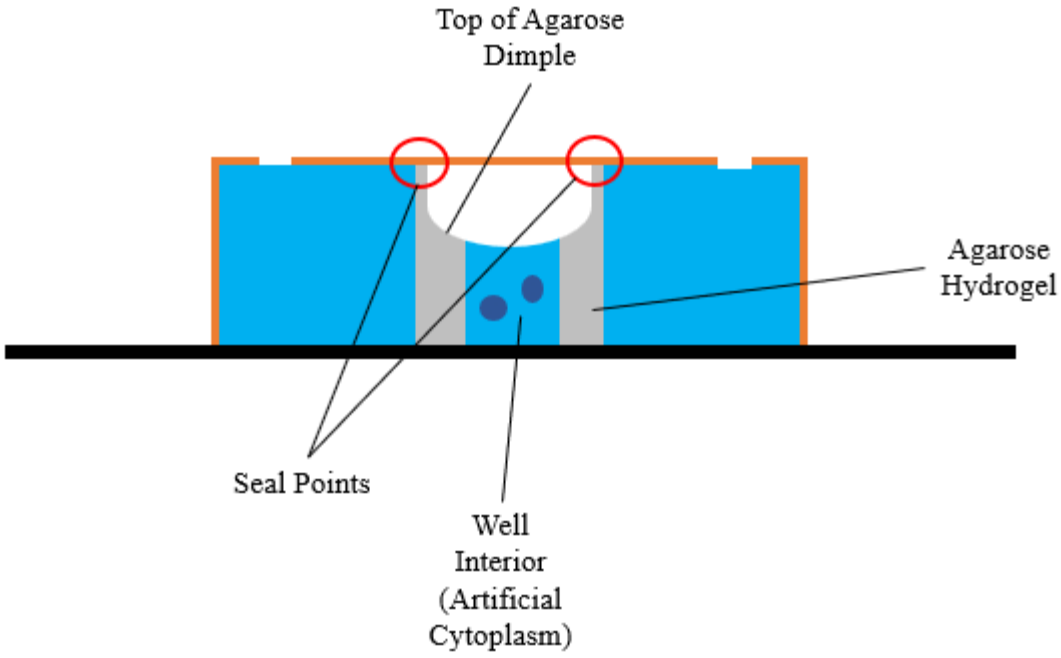

Figure 5. Side view diagram depicting the contact particle seal demonstrated by the 2.05 mm tall agarose hydrogel. Contents of the well interior did not leave the well and particles outside of the seal points could not enter the sealed interior of the hydrogel. Since the entire hydrogel interior space was not filled with sample solution contents, air was sealed in the hydrogel interior also.

Due to the dimpled shape of the agarose hydrogels, the tallest outer portion of the hydrogel formed a contact seal with the cover of the perfusion chamber. Tracer particles were observed to be unable to cross through this seal. Since the well interior was filled with tracer particles in solution but the rest of the dimple was not filled, this sealed in excess air with the sample.

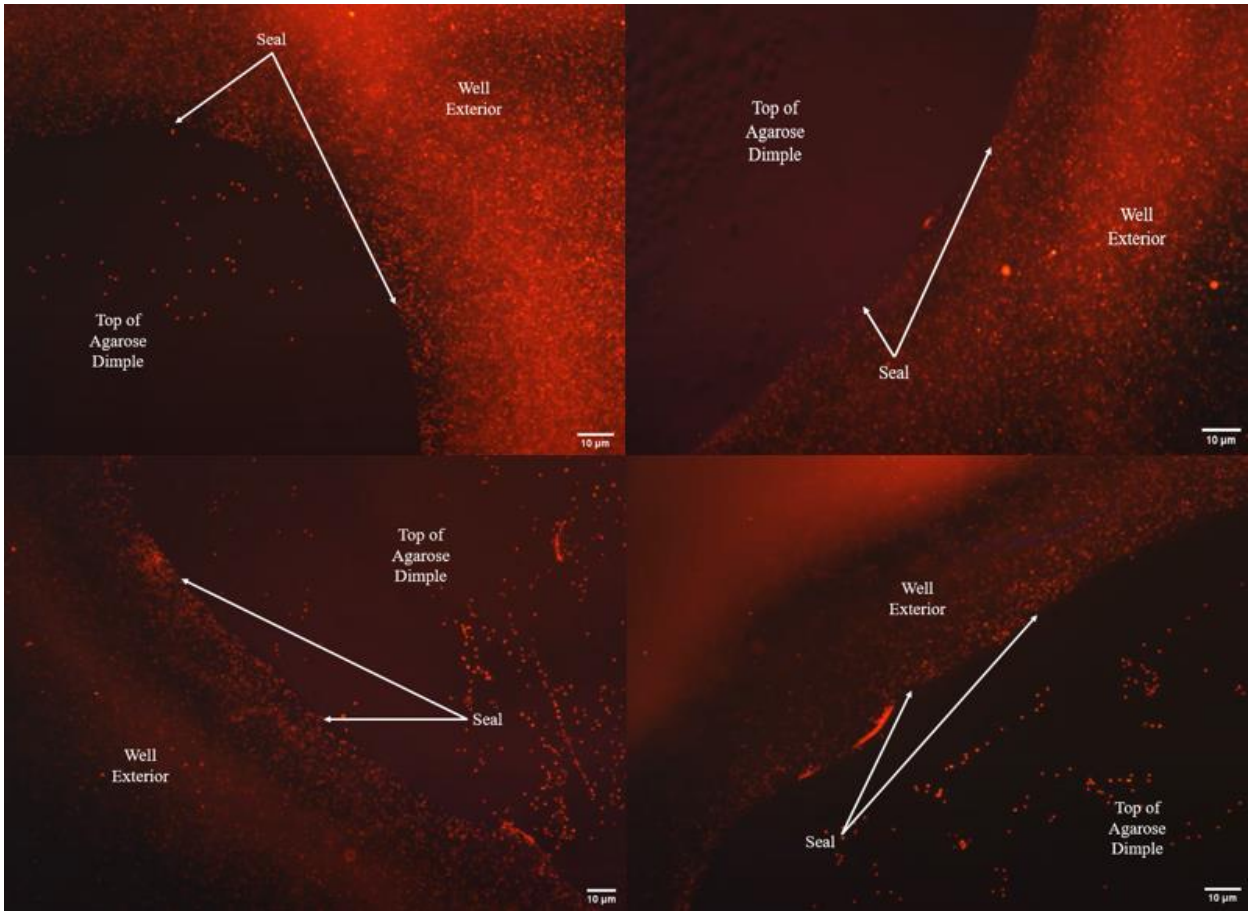

Figure 6. Fluorescent microscope image of the contact particle seal formed with a 2.05 mm tall agarose hydrogel using 10x magnification. Tracer particles in the exterior were unable to cross the contact seal. Particles on top of the agarose dimple were unmoving because there was no water here through which they could diffuse.

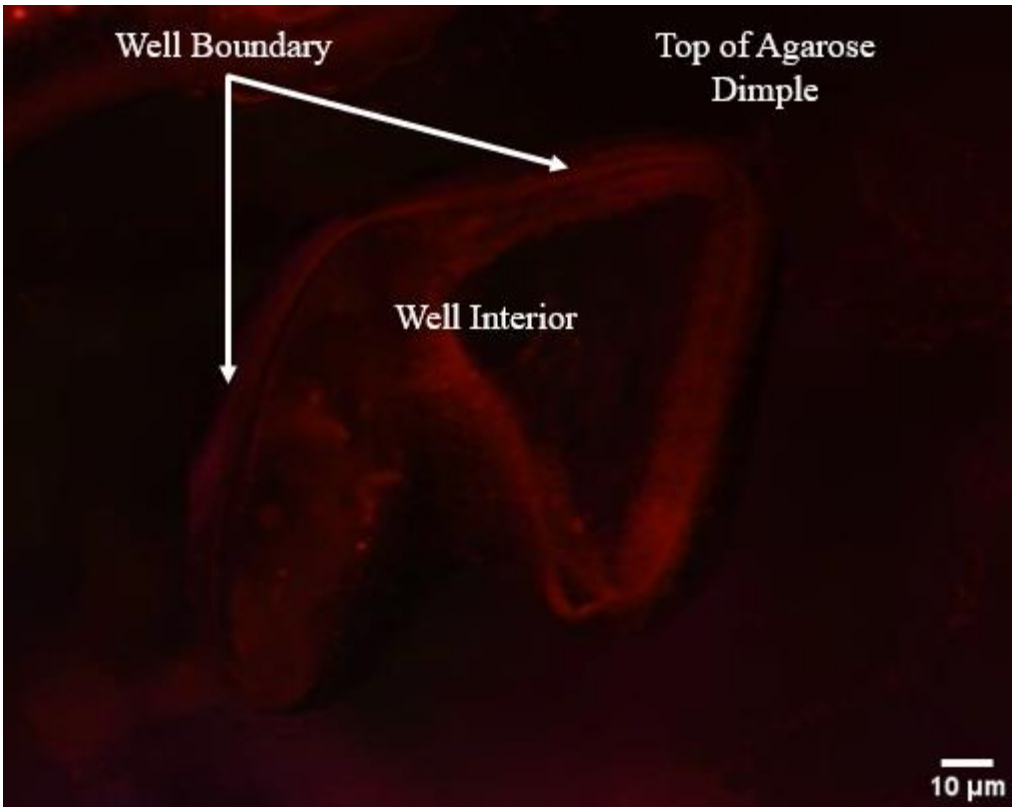

Figure 7a. Fluorescent microscope image of the well interior, sealed inside of the agarose hydrogel dimple using 4x magnification. Tracer particles were observed to passively diffuse within the boundaries of well interior. Well shape was cut out by hand using a scalpel.

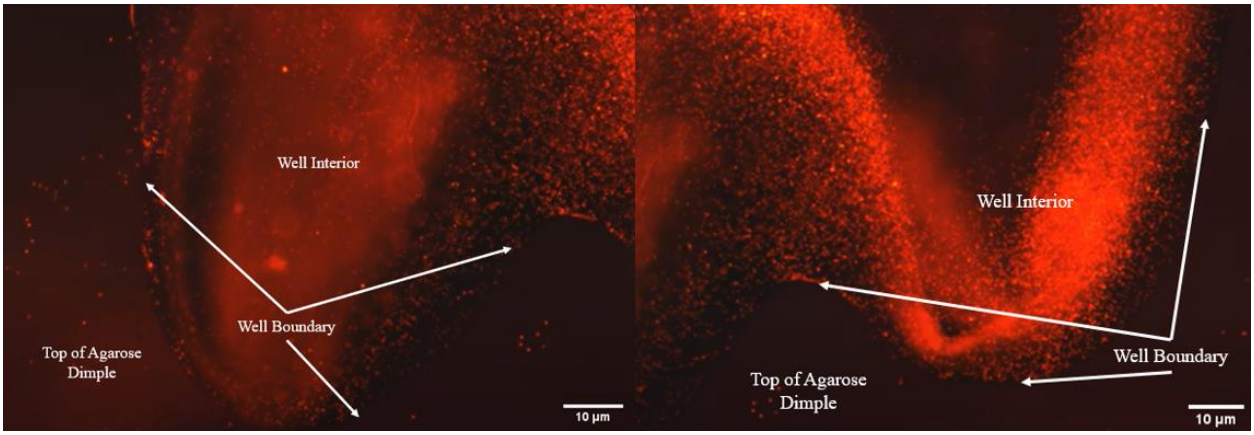

Figure 7b. Fluorescent microscope image of the well interior within the particle contact seal using 10x magnification. Tracer particles were observed to passively diffuse within the boundaries of the well interior.

Tracer particles are present in the well exterior because they leaked out of the well prior to it being sealed – no tracer particles were observed to leak through the contact seal formed **[Figure 6]**. Particles are also present on top of the agarose hydrogel dimple **[Figure 6** and **7a-b]** – these are present due to the way tracer particles were pipetted into the well interior. To find the well interior, the pipette tip full of tracer particles in solution needs to be used to feel around for the boundaries of the well. This necessarily releases some tracer particles on the top of the hydrogel dimple. Since there is no water here, these particles were observed to be motionless, as they did not have any medium to diffuse in.

7 DISCUSSION – DRIFT-REDUCING CHAMBER

7.1 SUMMARY OF RESULTS

The creation of the agarose hydrogel was successful, and the drift-reducing chamber with a 2.05 mm tall hydrogel formed a sealed space within the hydrogel interior. The taller edges of the hydrogel did not allow tracer particles past the contact seal formed and the tracer particles within the well interior remained there while retaining their diffusive motion.

7.2 CONTEXTUALIZATION OF RESULTS

Using a 2.05 mm tall agarose hydrogel, the outer tallest portion of the hydrogel contacted the cover of the perfusion chamber, sealing the interior of the agarose hydrogel from the excess exterior space. Tracer particles were unable to cross this seal that was formed. Based upon these results, it is possible to create a sealed well in which particle diffusion can be studied. Tracer particles within the well remained there and retained their diffusive motion, and tracer particles outside the hydrogel exterior could not move through the seal and enter the well. This seal is a promising result for future research attempting to construct a drift-reducing chamber that can allow for the avoidance of drift when constructing an artificial cell. These results also demonstrate that constructing this chamber may not require such an arduous process as Palacci (2010) previously described [8] – after determining what the dimensions of what the agarose hydrogel should be (2.05 mm for the Electron Microscopy Sciences perfusion chamber), a readily repeatable process can be undertaken to construct a sealed well within a drift-reducing chamber.

Although a seal was achieved in this study, there is more work that needs to be done to determine if the approach in this study is viable in its entirety. When the contact seal was formed, there was air that was sealed within the region above the well interior and in the dimple of the agarose hydrogel. It is expected that water would diffuse through the hydrogel and into this region, removing the air here by forcing it to diffuse out. However, this did not occur and the air within the seal remained. It is hypothesized that since there was no further water introduced to the system, the osmotic pressure present in both the hydrogel interior and exterior reached an equilibrium, where the osmosis of water through the hydrogel came to a standstill. However, it may be that when more water is introduced to the system, the osmotic pressure in the hydrogel exterior could increase such that the water diffuses through the hydrogel and pushes the excess air from the interior out through the hydrogel as a result. The next test for future studies is to flow fluorescently dyed water into the chamber and to observe what happens with this osmosis of water. Based on Palacci's work [8] and the properties of agarose hydrogels, it is expected that the water will diffuse through the hydrogel in the presence of an osmotic pressure gradient. However, it is not a given that this will be observed with the approach in this study, and future studies interested in using a drift-reducing chamber would find this worthwhile to investigate.

7.3 Drift-Reducing Chamber Difficulties

Construction of the drift-reducing chamber prototypes were optimized through testing. One method that was optimized was the hydrogel mold that would be most effective. At first, the perfusion chamber itself was used by overfilling the space in a separate perfusion chamber with the hot liquid hydrogel. The idea behind this method was to make use of the hydrogel's ability to plastically deform to create an effective seal inside the chamber. However, this method produced a

hydrogel that was far too tall for the chamber's interior because the hydrogel had a convex meniscus when it set. The next attempt was made with the perfusion chamber once again, but a glass slide was used to scrape excess liquid hydrogel from the top of the mold. However, these hydrogels came out too short and floated within the perfusion chamber, allowing tracer particles to leak out from the well.

Due to the inefficacy of these procedures, a different approach was attempted using more precise measurements. Using a caliper, the depth of the perfusion chamber was measured to be 1.65 mm. From this measurement, cylindrical plastic molds were made with specific depths varying around 1.65 mm to find the hydrogel height that would effectively seal the well interior. These molds, depicted in **Figure 3a-b**, were made using a drill press bit with a specified diameter D, and were drilled to a specified depth, h. Despite the measurement made with the caliper, it was found that a hydrogel with a height of 1.65 mm was far too small to effectively seal in the chamber, despite precise measurement of the chamber depth. The cause of this discrepancy was due to the curvature of the well bottom, which was caused by the technique used to drill into the plastic without melting it, combined with the trimming of the hydrogel edges when the gels turned out to be too large to fit within the confines of the perfusion chamber.

The optimal molds were found to be the molds made with a diameter $D = 0.50$ inches, which fit inside the perfusion chamber without any trimming necessary. The quality of the chamber was increased immediately, with a 1.65 mm tall hydrogel demonstrating some areas of the boundary sealed – however, there was still a leak through the seal that was visible at this height, depicted in **Figure 8**. A similar result was found using hydrogels that were 1.75 mm and 1.85 mm tall, but no leaks were found using a 2.05 mm hydrogel. The requirement for a hydrogel that is taller than the depth of the perfusion chamber is thought to be due to the increase in pressure of the hydrogel

pushing against the top cover of the perfusion chamber when forced to plastically deform – this increase in pressure may make a stronger seal that does not allow any tracer particles to pass through.

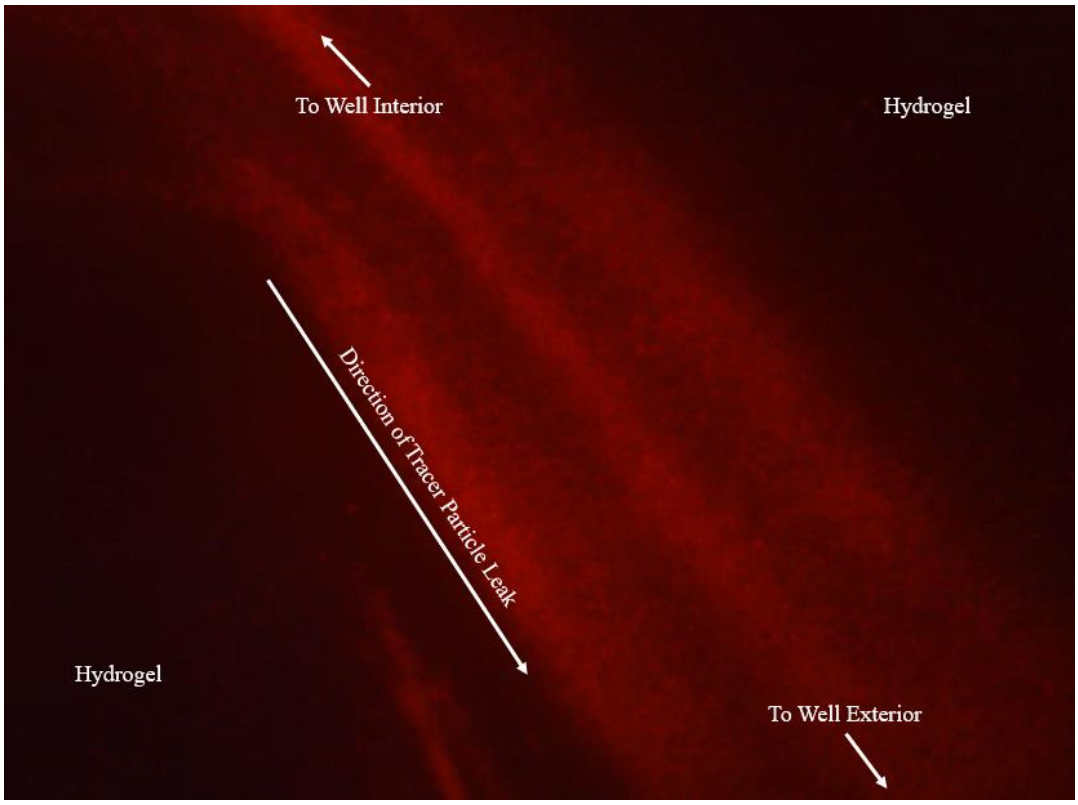

Figure 8. Fluorescent microscope image taken from a video of tracer particles flowing out of a hole in the seal at the well boundary through a hydrogel of height 1.65 mm. Video was captured using 10x magnification.

8 EXPERIMENTAL DESIGN – TRACER DIFFUSION

8.1 SAMPLE SLIDE OVERVIEW

Sealed sample chamber slides were used to analyze the passive diffusion of fluorescently dyed sulfate latex tracer particles (Fluoromax, 1.1 μm diameter) in aqueous environments containing various concentrations and polymer chain lengths of PEG. A droplet of aqueous solution containing the PEG dilution and tracer particles was pipetted into a larger droplet of olive oil, and this sample was sealed between two coverslips with a secure seal spacer (Electron Microscopy Sciences) of 9 mm diameter to reduce drift in the sample **[Figure 9a-b]**. Sealed slides were chosen for this study to isolate the tracer particle environment from the outside. Previous research has used open-top slides when analyzing fueled Janus particle motion to allow molecular oxygen to escape [1]; however, tracer particles do not produce this molecular oxygen byproduct and can safely be analyzed in an enclosed space.

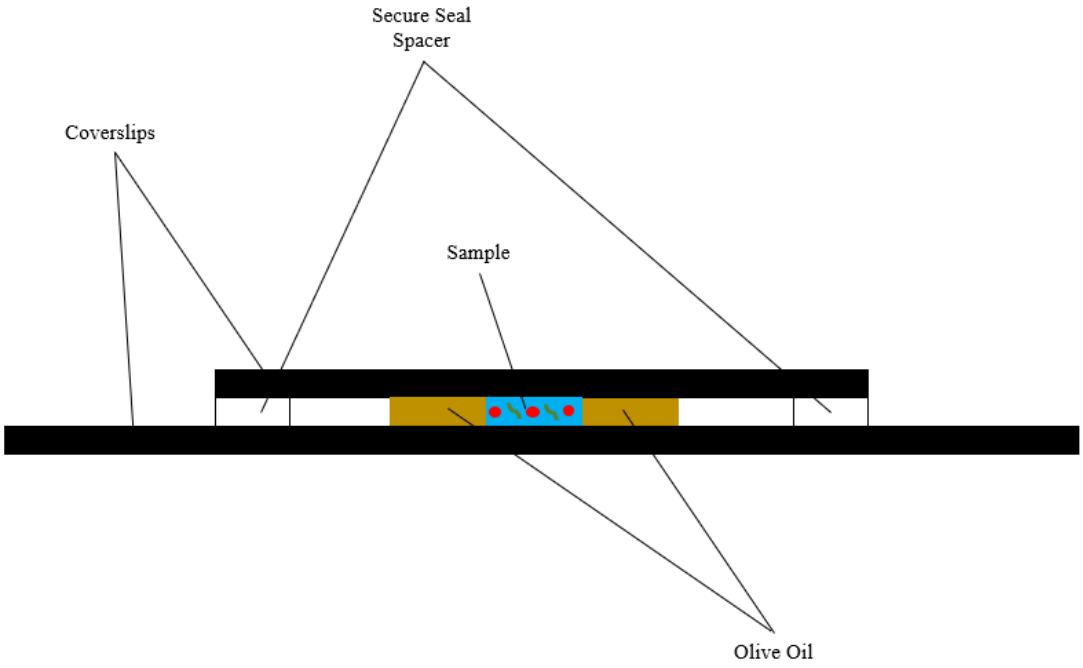

Figure 9a. Side view of the sealed sample chamber slides used to study the diffusion of tracer particles. A secure seal spacer was secured to the bottom coverslip, the sample solution was pipetted into an olive oil droplet in the sample well, and a second coverslip was secured to the top of the secure seal spacer to seal the well from the external environment. [Not to scale]

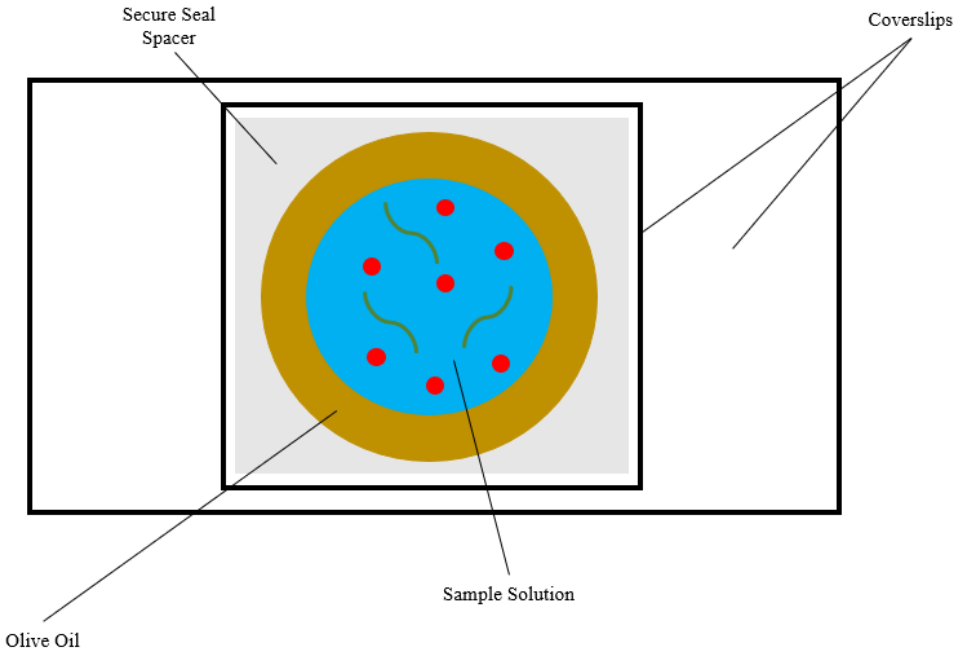

Figure 9b. Top-down view of the droplet-in-oil configuration used to study tracer particle diffusion. Pictured is an aqueous sample solution (blue) with tracer particles (red) and PEG (green) inside a larger droplet of olive oil (brown). [Not to scale]

Tracer particle motion was captured using fluorescence microscopy with a Nikon Ti-E Inverted Microscope and a ThorLabs color camera, recording data at 17.29 fps. Analysis was performed using TrackPy software [15]

8.2 METHODS

Tracer particle samples were prepared by placing a secure seal spacer on a single coverslip, creating an open well where the droplet-in-oil configuration would be located. 4 μL of olive oil was first pipetted into the well. In an Eppendorf tube, 1 μL each of RO water, PEG of a desired concentration (10 mg/mL, 20 mg/mL, 30 mg/mL, 40 mg/mL, or 50 mg/mL) and polymer chain length (200, 2000, 8000, or 20000), and recently vortexed tracer particles were added and vortexed to thoroughly mix the solution. The contents of the Eppendorf tube were pipetted into the olive oil in the sample well, creating the droplet-in-oil configuration depicted in **Figure 9b**. This configuration was used to reduce drift produced from evaporative effects. The sample was sealed by placing another coverslip on top of the sample well.

Once the sample slide was sealed, the slide was imaged using fluorescence microscopy and recorded by a camera using 40x magnification. After the video was recorded, it was split into three sections of roughly equal length and each section was analyzed using TrackPy software [15] to estimate the spread in the diffusion parameters throughout the duration of the captured video. Both the general diffusion coefficient and the diffusive exponent were determined using this software. This entire process was repeated for tracer particles in aqueous solutions containing every combination of PEG concentration and PEG polymer chain length using the aforementioned choices.

9 RESULTS – TRACER DIFFUSION

9.1 LOG PLOTS AND MSD PLOTS

In aqueous dilutions with all possible combinations of selected PEG concentrations and PEG polymer chain lengths, TrackPy [15] analyzed the diffusion of tracer particles. This software determined the trajectories of individual particles, demonstrated in **Figure 10**.

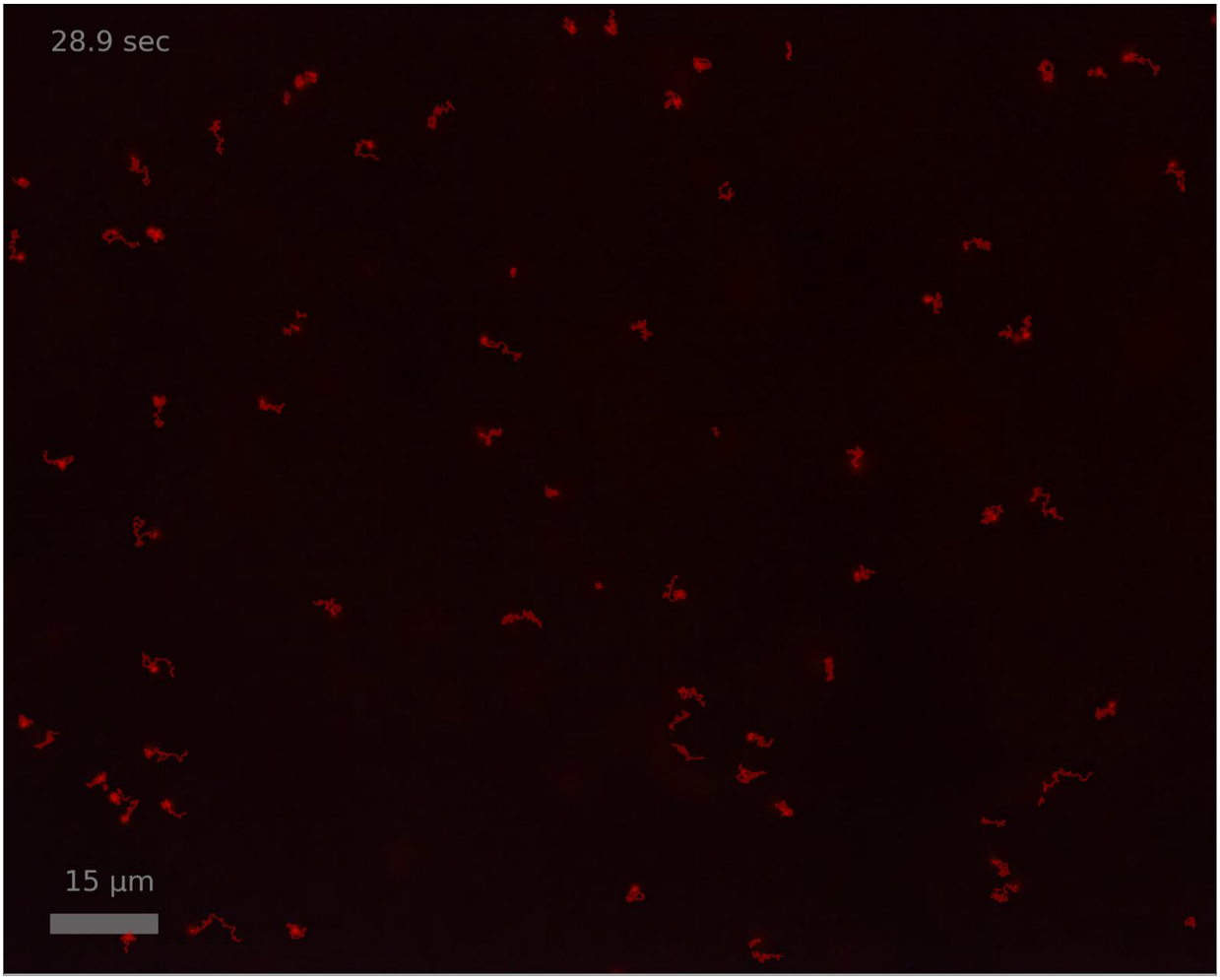

Figure 10. An example of tracer particle trajectories determined by the TrackPy software [15]. Image is from the analysis of tracer particle diffusion in aqueous solution of PEG 8000 at 40 mg/mL.

Using these trajectories, the software then made plots of MSD versus time **[Figure 11a-d** and **Figure 12a-e]**. **Figure 11a-d** is a collection of these MSD plots for all three video segments at each PEG concentration. As the PEG concentration increases, the slope of the MSD versus time plot generally decreased. Additionally, plots of MSD versus time are shown in **Figure 12a-e** for various PEG polymer chain lengths at a fixed PEG concentration. Generally, as the polymer chain length increased, the slope of the MSD plot decreased.

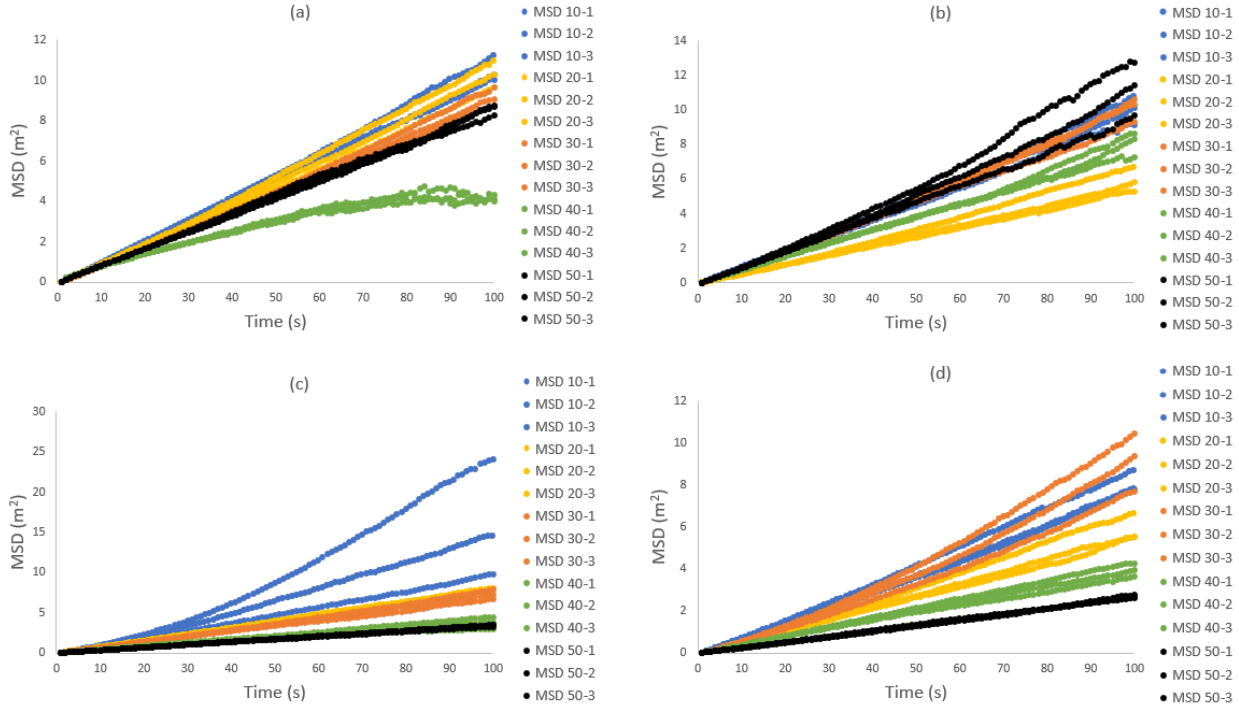

Figure 11. MSD (m^2) versus time (s) plots for various PEG polymer chain lengths: **(a)** PEG 200; **(b)** PEG 2000; **(c)** PEG 8000; and **(d)** PEG 20000. Legends are labeled by PEG concentration (10, 20, 30, 40, or 50) in mg/mL and numbered video segment (1, 2, or 3).

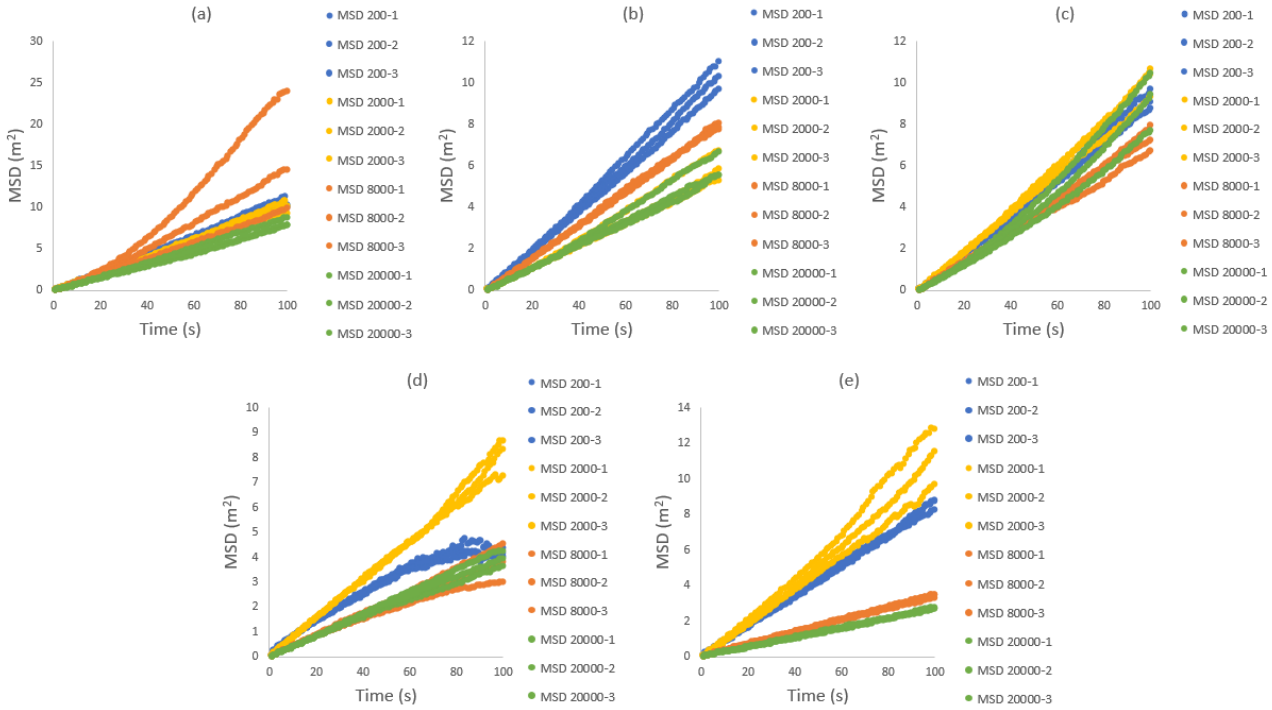

Figure 12. MSD (m^2) versus time (s) plots for various PEG concentrations: **(a)** 10 mg/mL; **(b)** 20 mg/mL; **(c)** 30 mg/mL; **(d)** 40 mg/mL; and **(e)** 50 mg/mL. Legends are labeled by PEG polymer chain length (200, 2000, 8000, or 20000) and numbered video segment (1, 2, or 3).

The MSD plots in **Figure 11a-d** and **Figure 12a-e** mostly demonstrated linearity. The software used is programmed to take advantage of this and make log plots of MSD versus time. Log plots were advantageous for this study due to the linear nature of the plots of the logarithm of MSD versus the logarithm of time for the videos analyzed. Thus, by taking the logarithm of both sides of **Equation 10** and using logarithm rules,

$$\log\langle r^2\rangle = \alpha \log t + \log(6D) \tag{11}$$

where α is both the diffusive exponent and the slope of the log plot, and $\log(6D)$ is the y-intercept of the log plot. From these, the software can calculate the diffusive exponent and diffusion coefficient. It should be noted that the software used in this study determines a general diffusion coefficient, A, which is a number that does not consider any numerical factors that are used to

determine the true diffusion coefficient in the Einstein and the Stokes-Einstein relations. Since the videos record only two dimensions of motion, the coefficient measured in this study is four times the true diffusion coefficient found in the Einstein relation, making the equation of the log plots

$$\log\langle r^2\rangle = \alpha \log t + \log(A) \tag{12}$$

such that $A = 4D$. Nonetheless, this difference does not change the validity of the general diffusion coefficients measured in this study as analogs for the true diffusion coefficient, as this measured coefficient directly depends on the true coefficient.

9.2 Measured Diffusion Coefficients and Diffusive Exponents

Figure 13a-d is a collection of plots of the measured general diffusion coefficients for tracer particles in aqueous dilutions of PEG with polymer chain lengths of 200, 2000, 8000, or 20000. The error bars are estimated from the range in measurements from each of the three video sections. Except for PEG 2000, the general diffusion coefficient predominantly decreased with an increased concentration of PEG **[Figure 13a-d]**.

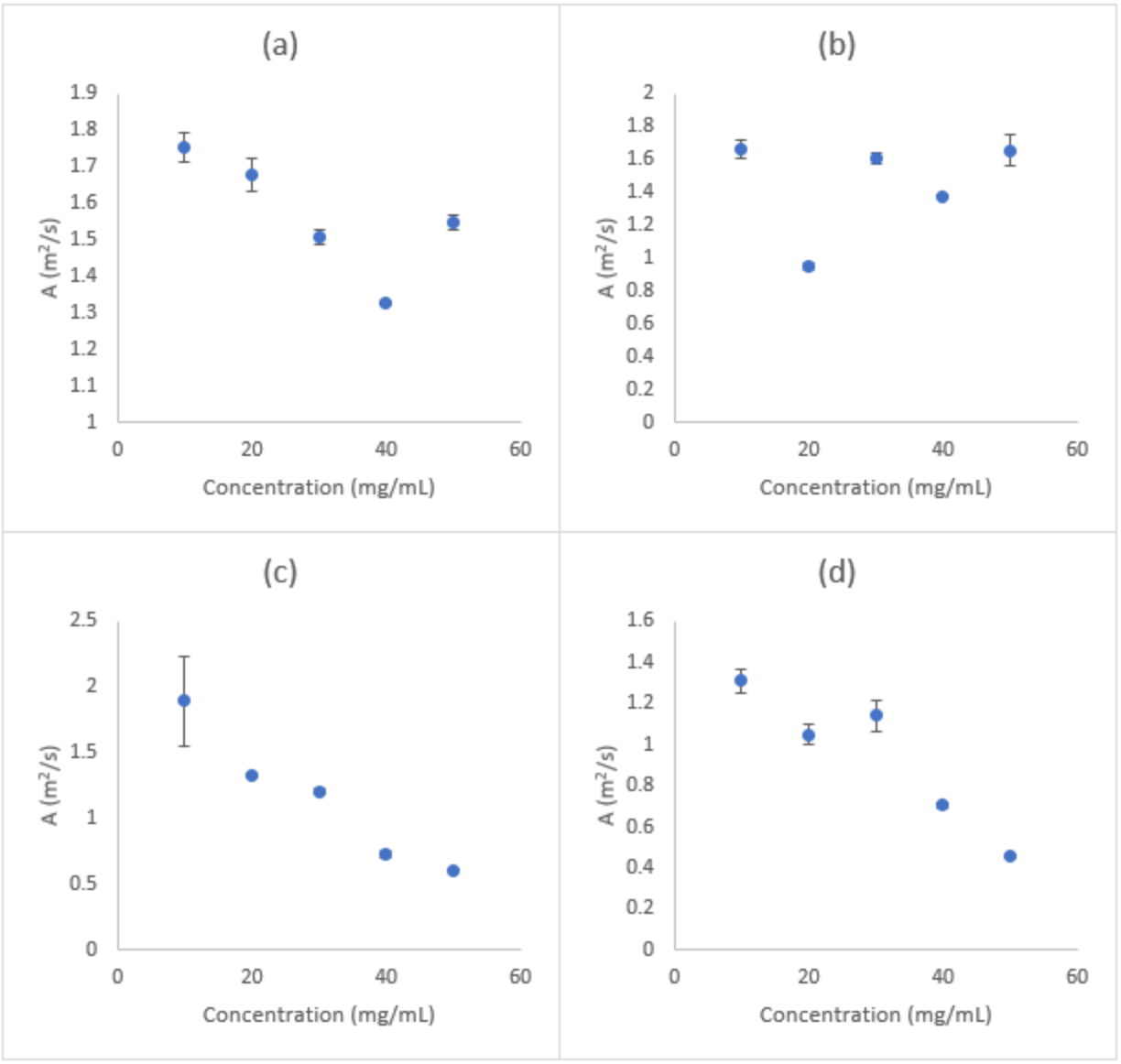

Figure 13. Measured general diffusion coefficient (m^2/s) versus PEG concentration (mg/mL) for tracer particles in aqueous dilutions of various PEG polymer chain lengths: **(a)** PEG 200; **(b)** PEG 2000; **(c)** PEG 8000; and **(d)** PEG 20000.

To compare the motion of different polymer chain lengths, an overlaid plot of the measured general diffusion coefficient versus PEG concentration for tracer particles in all PEG polymer chain lengths demonstrates the variations between different conditions **[Figure 14]**. Generally, as the PEG polymer chain length increased, the general diffusion coefficient decreased.

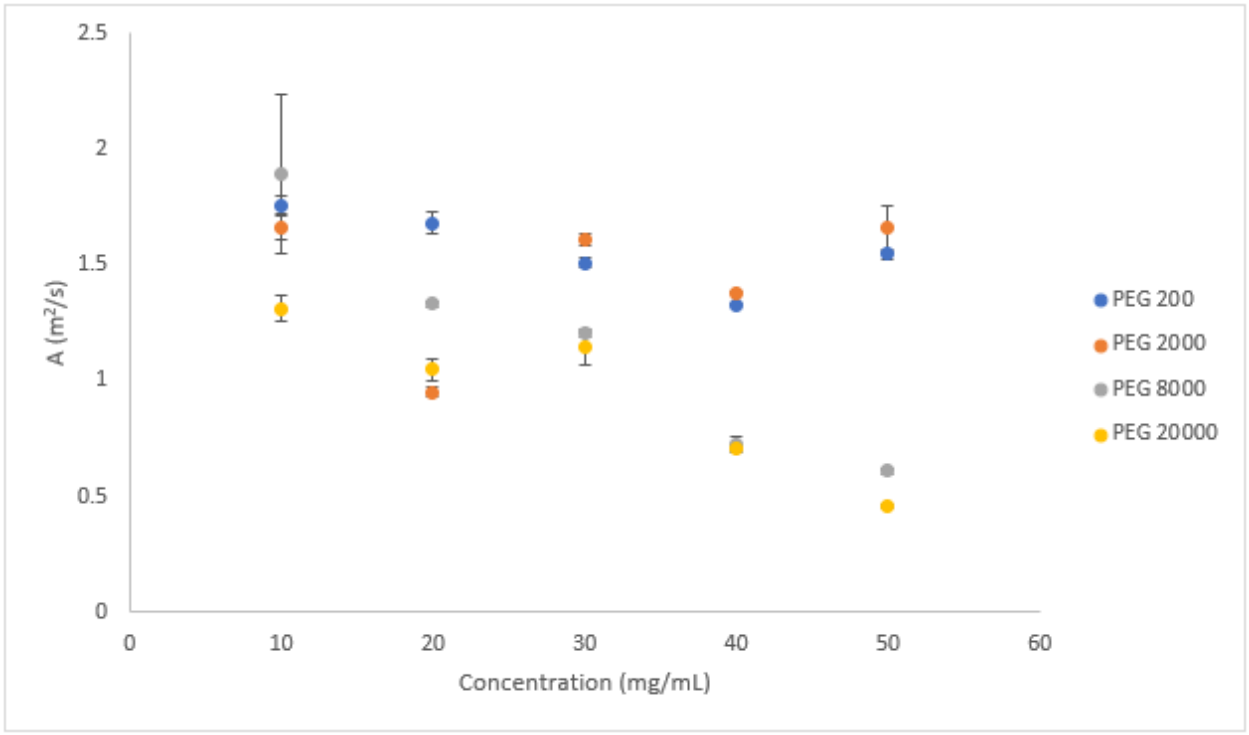

Figure 14. Overlay of all measured general diffusion coefficient (m^2/s) versus PEG concentration (mg/mL) plots for tracer particles in various aqueous PEG dilutions.

Figure 15a-d is a collection of plots of the diffusive exponent (α) versus PEG concentration for tracer particles in aqueous dilutions of PEG 200, 2000, 8000, and 20000. **Figure 16** is an overlay of all diffusive exponent values (α) versus PEG concentration plots across all studied PEG polymer chain lengths. The diffusive exponent generally remained constant no matter the differences in PEG concentration or PEG polymer chain length at $\alpha \approx 1$.

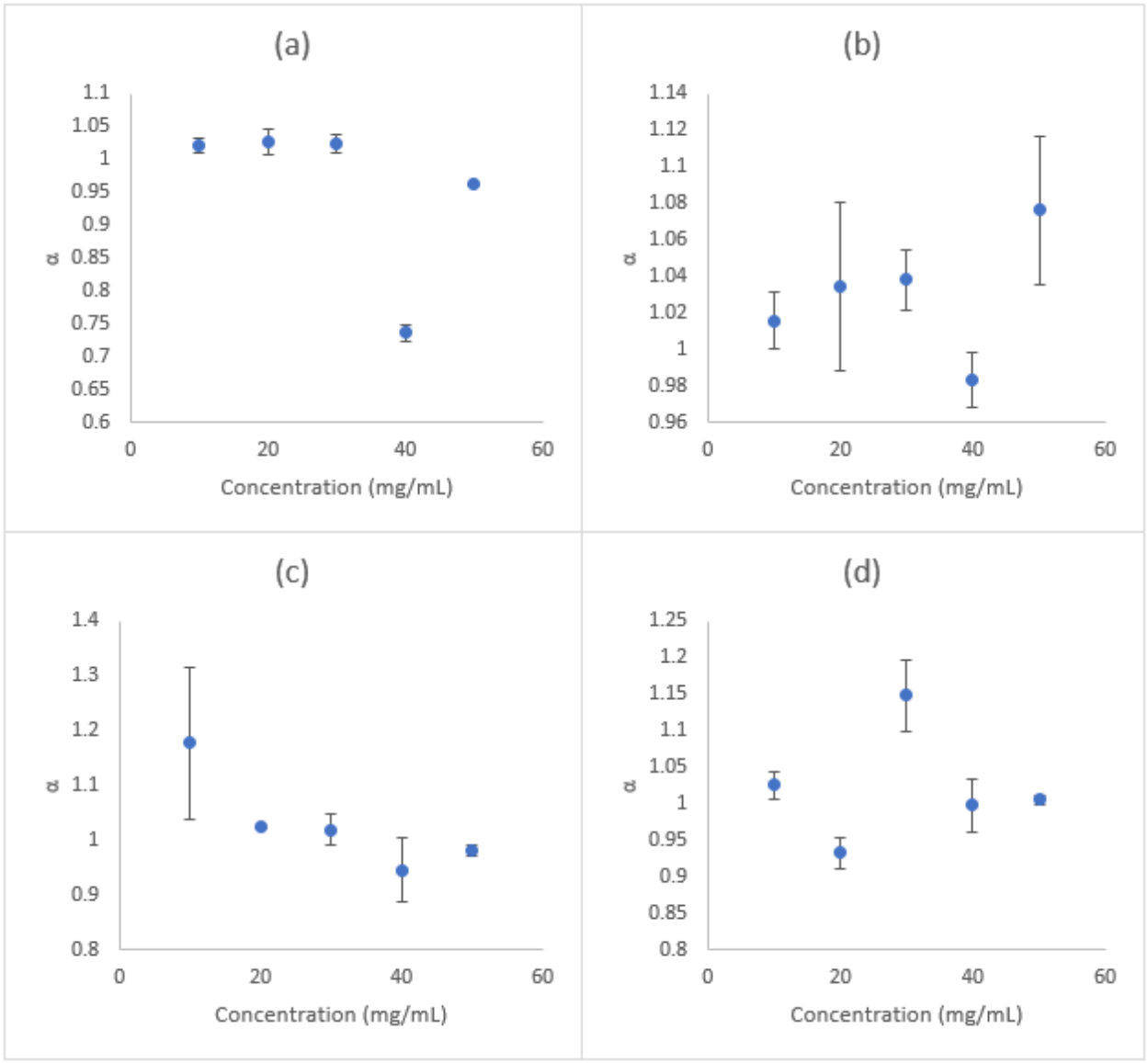

Figure 15. Diffusive exponent (α) versus PEG concentration (mg/mL) for tracer particles in aqueous dilutions of various PEG polymer chain lengths: **(a)** PEG 200; **(b)** PEG 2000; **(c)** PEG 8000; and **(d)** PEG 20000.

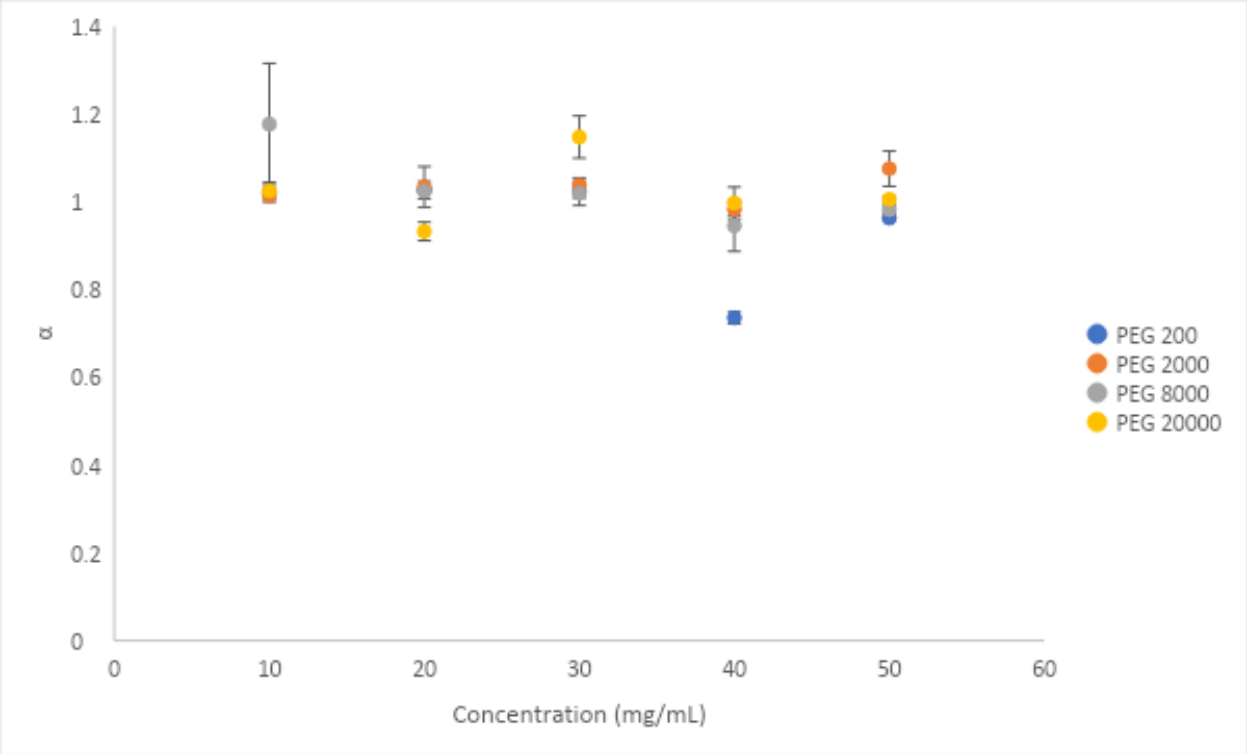

Figure 16. Overlay of all diffusive exponent values (α) versus PEG concentration (mg/mL) for tracer particles in various aqueous PEG dilutions.

Since the diffusive exponents were all measured to be roughly $\alpha = 1$, it will be assumed that the diffusive exponent truly is $\alpha = 1$ for these samples. As such, the slopes of the MSD plots in **Figure 11a-d** and **Figure 12a-e** are the measured general diffusion coefficients. Both for increasing PEG concentration and increasing PEG polymer chain length, the slopes of the MSD plots generally decreased **[Figure 11a-d** and **Figure 12a-e]**. This trend in MSD plot slopes reinforces the result that the measured general diffusion coefficient decreased with increasing PEG concentration **[Figure 13a-d]** and with increasing PEG polymer chain length **[Figure 14]**.

10 DISCUSSION – TRACER DIFFUSION

10.1 SUMMARY OF RESULTS

The analysis of tracer particle diffusion demonstrated that with an increased PEG concentration, the measured general diffusion coefficient decreased. With an increased PEG polymer chain length, the measured general diffusion coefficient also decreased. Additionally, the diffusive exponent remained roughly constant at $\alpha = 1$ regardless of any variations in PEG concentration or polymer chain length. Plots of MSD versus time mostly demonstrated linearity, providing rationale alongside the experimental measurements of the diffusive coefficient for the assumption that $\alpha = 1$ for the samples analyzed in this study. Thus, for the rest of this discussion, it will be assumed that the diffusive exponent's true value throughout these experiments was exactly one to speculate further regarding the general diffusion coefficient results.

10.2 CONTEXTUALIZATION OF RESULTS – TRACER DIFFUSION

The results of this study demonstrated that the diffusion coefficient is dependent upon the crowdedness of the diffusive medium. An increased concentration of PEG correlated with this decrease in the diffusion coefficient, and it is reasonable to assume that this trend would be observed with other organic molecules or biomolecules. PEG is an organic polymer with a long chain structure, much like the tails of biomolecules such as various types of lipids. The environment of the samples in the present study was aqueous as well, much like the intracellular environment.

The diffusion coefficient also depends upon the bulkiness of the molecules in the medium as well, as longer PEG polymer chain lengths corresponded to smaller diffusion coefficients at the

same concentration. Many biomolecules present in the intracellular environment are large – one example being titin, one of the largest known proteins with a peptide chain of 34,000 amino acids [16]. The PEG polymers used in this study have sizes on the order of nanometers [17], similar to the sizes of many proteins [18], demonstrating that the PEG molecules used in this study span a size range that is comparable to that of biomolecules that appear within biological cells. Thus, it is likely that these results regarding solute bulk would apply to the passive diffusion observed in intracellular environments. As demonstrated by the Stokes-Einstein relation in **Equation 9**, the difference between the measured diffusion coefficients is likely due to variations in medium viscosities that stem from the differences in PEG polymer chain lengths used [13]. Gonzalez-Tello et al. (1994) [19] has analyzed the viscosities of various PEG polymer chain lengths in aqueous solution, determining that as average molecular mass increases (corresponding to an increase in polymer chain length), the viscosity of the corresponding aqueous solution decreases. Thus, sample media containing longer PEG polymer chain lengths would correspond with larger medium viscosities, and due to the inverse proportionality between the diffusion coefficient and solution viscosity [13], smaller diffusion coefficients would be expected for tracer particle diffusion in these samples. This is the general result that was observed in this study.

While the diffusion coefficient changed with variation in PEG concentration and polymer chain length, the diffusive exponent remained roughly constant at $\alpha = 1$. Additionally, plots of MSD versus time were mostly linear. Since the tracer particles were passively diffusing in this study, this experimentally reaffirms that passive diffusion yields a diffusive exponent of $\alpha = 1$ [1, 14], also demonstrating the accuracy of the theoretically derived Einstein relation [13]. Furthermore, the constancy in the diffusive exponent is important because it demonstrates a clear difference from the fueled motion of Janus particles [1, 9]. Horowitz et al. (2019) [1] and Howse et al. (2007) [9] determined that the fueled motion of self-propelling Janus particles resulted in an increased diffusive

exponent, characteristic of superdiffusion [1, 14]. Therefore, medium crowdedness and fueled motion independently affect two different parameters, and the causes of any changes in motion may be determined by analyzing a particular particle's motion and parsing out which parameter (either the diffusion coefficient or diffusive exponent) changed from its value outside of the medium in question. Additionally, decreases in the diffusive exponent may not be due to the crowdedness of the medium, as subdiffusive motion was only observed in one sample and was likely an erroneous data point for reasons that will be addressed in **Section 10.3**. Thus, subdiffusive motion could exist due to another characteristic of the medium – however, this cannot be confirmed without the analysis of tracer particle diffusion in media with higher concentrations of PEG than those used in this study to determine if these observed results are generalizable to all cases. With these results, future studies can analyze particle motion in biological cells and determine if the motion is energetically powered, hindered by a crowded medium, both, or some other combination altogether.

10.3 Sources of Error and Their Treatment

Among the many sources of error in the current study, the most significant was ensemble drift, which refers to a general group motion of all particles in a sample. Sealed slides were used for the tracer particle diffusion section of this study to isolate the samples from an external environment. However, this only does so much – at times, the entire sample can be characterized by extreme amounts of ensemble drift for any number of reasons, making it unusable due to its potential to skew the diffusion parameters measured. Large amounts of ensemble drift are observable by eye after some practice and when observed within a sample, the sample was disposed of and a new one was made, until the ensemble drift was reasonable.

Even when watching for it, there can still be drift that is imperceptible by eye. To account for this, Horowitz et al. (2019) [1] used a TrackPy script [15] that corrected for the drift using a technique involving singular value decomposition. This TrackPy script [15] was used in the current study as well in an attempt to increase the accuracy of the measurements made. Additionally, the droplet-in-oil configuration within the sealed slides was used to stop evaporative effects within the sample, as evaporation contributes to the production of drift (although these effects are considered to be minor in the case of a sealed sample) [1].

In the plots for MSD versus time **[Figure 11a-d** and **Figure 12a-e]**, some plots deviated from the typical linear behavior that governed most samples. This is characteristic of anomalous diffusion [14] and when compared to the rest of the data collected, these few plots do not logically fit the rest of this study's observations. Anomalous diffusion was only observed in a few instances – subdiffusion was observed in all videos for one sample of tracer particles in PEG 200 at 40 mg/mL (with average $\alpha = 0.736 \pm 0.013$), and superdiffusion was only observed in a few samples, such as one of the videos for PEG 8000 at 10 mg/mL (with $\alpha = 1.32$). Since cases of anomalous diffusion such as these few examples were in the vast minority, it is very likely that these few samples had tracer particle motion affected by any number of sources of error, such as ensemble drift that could not be accounted for, an increased temperature due to remaining under the microscope lamp for longer than other samples, the movement of the sample over to the microscope too quickly, or potentially another unlisted source. It should also be noted that at longer time intervals, the MSD versus time plots demonstrate more noise because each of these MSD points are averages of the MSD of all tracer particles at that moment in time. Since it is not possible to track every particle for the entirety of the video (due to the particle moving out of the screen), the MSD average is performed over a decreasing number of points at longer time intervals, leading to noisier data in this range.

Estimates of error in measurements of the general diffusion coefficients and diffusive exponents were made based on the spread in measurements within one video. Each sample had a video length of roughly 500 frames, and these frames were split into three separate videos of roughly equal length. Both the general diffusion coefficient and diffusive exponent were measured for each of these three video sections, and the range of these measured parameters divided by two served as their error estimates.

10.4 A NOTE ON THE DIMENSIONS OF THE GENERAL DIFFUSION COEFFICIENT

Dimensions of the general diffusion coefficient can vary depending on the value of the diffusive exponent, which is determined by the specific type of diffusion observed – whether it be regular or anomalous. Since the diffusive exponent was assumed to be $\alpha = 1$ in correspondence with the Einstein relation because of the experimental results observed, the dimensions for the general diffusion coefficients measured in this study were identified as square meters per second.

11 FUTURE PATHS FOR RESEARCH AND CONCLUSION

11.1 FUTURE PATHS FOR RESEARCH

The results of this study can be built upon by future studies in conjunction with previously published findings to create an artificial cell in its entirety that can serve as a simplistic, yet adjustable model for a biological cell. If such an artificial cell were built, it would provide a finely tunable mock intracellular environment that could aid in studying the exact causes of biomolecular motion in the cytoplasm. The completion of the drift-reducing chamber would allow for an environment comparable to the intracellular environment through the avoidance of excess drift from external causes, while allowing for the self-propulsion of Janus particles. It would then be possible to study fueled motion in a crowded medium artificially, which would mean a controllable, simplified environment akin to that of a biological cell. This hypothetical apparatus could also enable the study of the effects of coupling by including inert tracer particles and fueled Janus particles within the same medium.

11.2 CONCLUSION

Using a perfusion chamber, glass slide, and an agarose hydrogel, it was determined that a sealed well can be formed using a 2.05 mm hydrogel with the equipment used in this study. This is a promising result, as it demonstrates that it may very well be possible to construct an artificial cell that avoids drift while including fueled motion that artificially mimics the types of biomolecular motion in the cytoplasm. Additionally, tracer particle diffusion was measured in aqueous media containing various combinations of PEG concentrations and PEG polymer chain lengths. It was found that the measured diffusion coefficient analog decreased with both an increase in PEG

concentration and an increase in PEG polymer chain lengths. Using the Stokes-Einstein relation, these results suggest that this change in diffusive motion derives from a change in the medium's viscosity. The results observed in this study indicate an exciting future for the artificial cells project, as they provide insight into two areas of the project that are necessary to achieve the construction of an entire artificial cell.

12 REFERENCES

1. Horowitz, V.R., et al., *Active colloidal particles in emulsion droplets: a model system for the cytoplasm.* The European Physical Journal Special Topics, 2019. **227**(17): p. 2413-2424.
2. van Megen, W. and S.M. Underwood, *Tracer diffusion in concentrated colloidal dispersions. III. Mean squared displacements and self-diffusion coefficients.* The Journal of Chemical Physics, 1989. **91**(1): p. 552-559.
3. van Beijeren, H., K.W. Kehr, and R. Kutner, *Diffusion in concentrated lattice gases. III. Tracer diffusion on a one-dimensional lattice.* Physical Review B, 1983. **28**(10): p. 5711-5723.
4. Kehr, K.W., K. Binder, and S.M. Reulein, *Mobility, interdiffusion, and tracer diffusion in lattice-gas models of two-component alloys.* Physical Review B, 1989. **39**(8): p. 4891-4910.
5. Pathria, R.K. and P.D. Beale, *12 - Phase Transitions: Criticality, Universality, and Scaling*, in *Statistical Mechanics (Third Edition)*, R.K. Pathria and P.D. Beale, Editors. 2011, Academic Press: Boston. p. 401-469.
6. Leptos, K.C., et al., *Dynamics of Enhanced Tracer Diffusion in Suspensions of Swimming Eukaryotic Microorganisms.* Physical Review Letters, 2009. **103**(19): p. 198103.
7. Luby-Phelps, K., et al., *Hindered diffusion of inert tracer particles in the cytoplasm of mouse 3T3 cells.* Proc Natl Acad Sci U S A, 1987. **84**(14): p. 4910-3.
8. Palacci, J., *Manipulation of colloids by osmotic forces*. 2010, Université Claude Bernard-Lyon I.
9. Howse, J.R., et al., *Self-Motile Colloidal Particles: From Directed Propulsion to Random Walk.* Physical Review Letters, 2007. **99**(4): p. 048102.
10. Information, N.C.f.B., *PubChem Compound Summary for CID 134694962, Glycols polyethylene;Poly(ethylene glycol);PEG*. 2022: PubChem.
11. Guo, M., et al., *Probing the Stochastic, Motor-Driven Properties of the Cytoplasm Using Force Spectrum Microscopy.* Cell, 2014. **158**(4): p. 822-832.
12. Schroeder, D.V., *An introduction to thermal physics*. 2000, San Francisco, CA: Addison Wesley.
13. Einstein, A., *Investigations on the Theory of the Brownian Movement*. 1956: Dover Publications, INC.
14. Banks, D.S. and C. Fradin, *Anomalous Diffusion of Proteins Due to Molecular Crowding.* Biophysical Journal, 2005. **89**(5): p. 2960-2971.
15. Allan, D., et al., *Trackpy v0.5.0*. 2021: Zenodo.
16. Goodsell, D. *Molecule of the Month: Titin*. 2015. DOI: 10.2210/rcsb_pdb/mom_2015_5.
17. Cruje, C. and D. Chithrani, *Polyethylene glycol density and length affects nanoparticle uptake by cancer cells.* J Nanomed Res, 2014. **1**(1): p. 27-32.
18. Schuck, P., et al., *Size-Distribution Analysis of Proteins by Analytical Ultracentrifugation: Strategies and Application to Model Systems.* Biophysical Journal, 2002. **82**(2): p. 1096-1111.
19. Gonzalez-Tello, P., F. Camacho, and G. Blazquez, *Density and Viscosity of Concentrated Aqueous Solutions of Polyethylene Glycol.* Journal of Chemical & Engineering Data, 1994. **39**(3): p. 611-614.

13 APPENDIX

Appendix 1. Experimentally determined diffusion coefficients and exponents of tracer particle diffusion in PEG 200.

Concentration (mg/mL)	Trial	A (m^2/s)	α
10	1	1.807312	1.034765
	2	1.722875	1.015657
	3	1.732741	1.015104
20	1	1.727214	1.046677
	2	1.635534	1.007133
	3	1.676388	1.028280
30	1	1.511035	1.021114
	2	1.528847	1.041270
	3	1.488282	1.011099
40	1	1.330192	0.723772
	2	1.331765	0.733971
	3	1.322462	0.750749
50	1	1.546373	0.963256
	2	1.567964	0.963094
	3	1.527387	0.964376

Appendix 2. Average experimentally determined diffusion coefficients and diffusive exponents of tracer particle diffusion in PEG 200 with uncertainties.

Concentration (mg/mL)	Average A (m^2/s)	Uncertainty in A (m^2/s)	Average α	Uncertainty in α
10	1.75	0.04	1.022	0.010
20	1.68	0.05	1.03	0.02
30	1.51	0.02	1.02	0.02
40	1.328	0.005	0.736	0.013
50	1.54	0.02	0.9636	0.0006

Appendix 3. Experimentally determined diffusion coefficients and diffusive exponents of tracer particle diffusion in PEG 2000.

Concentration (mg/mL)	Trial	A (m^2/s)	α
10	1	1.687967	1.031696
	2	1.706918	1.014473
	3	1.598703	1.000648
20	1	0.974574	1.089051
	2	0.947559	1.018683
	3	0.927955	0.996032
30	1	1.604015	1.048656
	2	1.580931	1.016325
	3	1.640081	1.049959
40	1	1.372461	0.981217
	2	1.382189	1.000152
	3	1.380562	0.969719
50	1	1.772661	1.112723
	2	1.625374	1.083745
	3	1.577204	1.032215

Appendix 4. Average experimentally determined diffusion coefficients and diffusive exponents of tracer particle diffusion in PEG 2000 with uncertainties.

Concentration (mg/mL)	Average A (m^2/s)	Uncertainty in A (m^2/s)	Average α	Uncertainty in α
10	1.66	0.05	1.02	0.02
20	0.95	0.02	1.03	0.05
30	1.61	0.03	1.04	0.02
40	1.378	0.005	0.98	0.02
50	1.65	0.10	1.08	0.04

Appendix 5. Experimentally determined diffusion coefficients and diffusive exponents of tracer particle diffusion in PEG 8000.

Concentration (mg/mL)	Trial	A (m^2/s)	α
10	1	1.864384	1.167968
	2	2.252697	1.321377
	3	1.563346	1.043952
20	1	1.322599	1.024561
	2	1.328851	1.024755
	3	1.347288	1.025326
30	1	1.178023	0.992360
	2	1.220013	1.020221
	3	1.219359	1.047314
40	1	0.701572	0.885122
	2	0.718842	0.951298
	3	0.761328	1.002222
50	1	0.601640	0.973104
	2	0.606257	0.993008
	3	0.621234	0.981784

Appendix 6. Average experimentally determined diffusion coefficients and diffusive exponents of tracer particle diffusion in PEG 8000 with uncertainties.

Concentration (mg/mL)	Average A (m^2/s)	Uncertainty in A (m^2/s)	Average α	Uncertainty in α
10	1.9	0.3	1.18	0.13
20	1.333	0.012	1.0249	0.0004
30	1.21	0.02	1.02	0.03
40	0.73	0.03	0.95	0.06
50	0.610	0.010	0.983	0.010

Appendix 7. Experimentally determined diffusion coefficients and diffusive exponents of tracer particle diffusion in PEG 20000.

Concentration (mg/mL)	Trial	A (m^2/s)	α
10	1	1.266466	1.010391
	2	1.377524	1.050270
	3	1.289735	1.015419
20	1	1.105418	0.955838
	2	1.030809	0.930350
	3	1.011266	0.913577
30	1	1.213743	1.194478
	2	1.148437	1.152914
	3	1.062531	1.097964
40	1	0.690617	0.960690
	2	0.716183	1.033501
	3	0.709760	0.999350
50	1	0.445915	1.012237
	2	0.457523	0.999819
	3	0.462507	1.007072

Appendix 8. Average experimentally determined diffusion coefficients and diffusive exponents of tracer particle diffusion in PEG 20000 with uncertainties.

Concentration (mg/mL)	Average A (m^2/s)	Uncertainty in A (m^2/s)	Average α	Uncertainty in α
10	1.31	0.06	1.03	0.02
20	1.05	0.05	0.93	0.02
30	1.14	0.08	1.15	0.05
40	0.706	0.012	1.00	0.03
50	0.455	0.008	1.006	0.006

Appendix 9. Data for MSD versus time for all videos of tracer particle diffusion in all PEG concentrations and PEG polymer chain lengths can be found at:

https://docs.google.com/spreadsheets/d/1Oe8f0ETcxe0fJxYqNBTK-ZwgInILyusd/edit?usp=share_link&ouid=117651873101843562882&rtpof=true&sd=true